



The critical state of crushable granular sand

Ke Shi¹ · Fan Zhu² · Jidong Zhao^{1,3}

Received: 13 October 2022 / Accepted: 13 October 2023 / Published online: 17 November 2023
© The Author(s), under exclusive licence to Springer-Verlag GmbH Germany, part of Springer Nature 2023

Abstract

The concept of critical state has been a cornerstone of modern critical state soil mechanics. It remains inconclusive how grain crushing affects critical state behavior in crushable granular sand. A multiscale computational approach is employed in this study to simulate the shearing behavior of crushable granular sand at critical state. Grain crushing is rigorously considered by preserving the co-evolutions of grain size and shape in the simulation of the shearing process. Systematic simulations on specimens with varying initial states and loading paths show unique characteristics of critical state for crushable granular sand in terms of critical state stress ratio, void ratio, breakage index, and shape descriptors which are independent of stress path and initial conditions. To further understand the deformation mechanisms of crushable sand at critical state, the volumetric strain is decomposed into three components due respectively to grain size reduction, the interlocking of irregular shaped grains generated by crushing, and inter-particle friction. Competing mechanisms among the three strain components are quantitatively analyzed and discussed. Initial void ratio and stress levels are found to play a prominent role in shaping the critical state deformation of crushable sand and such impact may be gauged through the fraction of grains that experience crushing.

Keywords Critical state · Deformation · Fabric anisotropy · Grain crushing · Peridynamics

1 Introduction

The classical critical state theory introduced by [40] and [42] builds the milestones in the development of soil mechanics. The classical definition for critical state of granular soil refers to a state in which the soil exhibits steady-state volumetric strain and deviatoric stress under sustained shear deformation. The soil behavior at the critical state can be described from various perspectives. Most commonly, a unique stress ratio, η_{cs} , as defined by the ratio of deviatoric stress and the mean principal stress, and a unique void ratio, e_{cs} , can be identified at the critical state.

A critical state line (CSL) can thus be defined in both q - p' and e - p' spaces. The position and shape of CSLs represent fundamental soil properties for interpreting soil testing data and constitutive modeling of soils. While the CSL in q - p' space is typically fitted by a straight line, exponential functions with empirical parameters are commonly adopted to delineate the CSL in e - p' space [16, 24, 50, 57]. Recently, the concept of critical state has been enriched by [26] who augmented the classical definition of critical state with additional conditions on fabric anisotropy. Current studies on granular soils now consider fabric evolution and fabric anisotropy using tools such as the X-ray tomography technique and micromechanics tools such as the discrete element method (DEM). Unique fabric characteristics are quantified by specific fabric tensors at critical state [10, 12, 13, 52, 60].

The critical state behavior of crushable granular soils remains less understood, as most existing studies on critical state assume that the granular soils are non-crushable or have negligible crushability. Both particle size and shape may undergo intensive changes for crushable soils when they are sheared toward large shear strains. This inevitably introduces complexity and challenge to the study of soil

✉ Jidong Zhao
jzhao@ust.hk

¹ Department of Civil and Environmental Engineering, Hong Kong University of Science and Technology, Hong Kong SAR, China

² Department of Urban Management, Kyoto University, Kyoto, Japan

³ HKUST Shenzhen-Hong Kong Collaborative Innovation Research Institute, Futian, Shenzhen, China

behavior and CSL profiles. While some studies have reported a limited influence of particle crushing on CSL in q - p' space [24, 57], others have confirmed that the increasing fine contents and interlocking effect due to successive grain crushing can raise the critical state friction angle of sands [14, 59]. The effect of particle crushing on the critical state void ratio is more controversial, due to the difficulty in tracking the evolving grading and CSL in e - p' space through laboratory tests. [1] have conducted a series of triaxial tests on sand samples reconstituted from the different initial states to track the CSL with varying degrees of breakage. A crushing-induced steeper CSL with a change in its intercept in e - p' space has been observed by various experimental and numerical studies [8, 9, 54, 56]. However, a consensus has not been reached on some critical aspects of CSL such as its specific form in e - p' space (e.g., nonlinear or bilinear) and the uniqueness of CSL with evolving grading. To quantify the degree of breakage, a grading index based on changes in particle size distribution curve has been incorporated, based on which the critical state surface (CSP) has been proposed to consider grading evolution due to particle crushing [6, 20, 33]. Moreover, the internal fabric of crushable sand at critical state remains to be explored due to the limited information on the evolution and critical state value of fabric anisotropy. Critical questions to be answered are, how the changing particle size and shape distribution give rise to an anisotropic contact network of an initially isotropic sand specimen, and whether a unique fabric anisotropy exists at critical state that satisfies the anisotropic critical state theory.

Particle crushing has a well-documented impact on the deformation of crushable soils. The consideration of grain crushing may critically affect the design and construction of various engineering structures such as driven pile installation and long-term settlement of foundations and dams [23]. Experimental observations indicate that particle crushing leads to a contractive behavior even at large shear strains and the constant volume at critical state is a balance of grain crushing and frictional rearrangement [9]. Further studies show that elevated confining pressure can also cause intensified crushing events, leading to transitional volumetric behavior from dilation to contraction [17, 28, 55]. There are more recent discussions on a possible competition between frictional dilation and crushing [7] and frictional dilation and shape-induced interlocking [27] during shearing deformation of granular materials. However, how grain crushing, friction, and interlocking effects reach an ultimate balanced state and the different contributions to overall sample deformation have not been rigorously validated by direct observations or quantitative analysis, either experimentally or numerically. It remains unclear how the different deformation mechanism, possibly including frictional dilation, crushing-induced contraction,

and shape-induced interlocking as mentioned before, interplay with each other to bring a crushable sand to critical state. It is ultimately desirable to fully revamp the classical critical state theory to include quantitative conditions of grain crushing to be suitable for crushable soils.

In most existing studies, the influence of grain crushing has been quantified by various breakage indices to account for evolving particle size, where the influence of particle shape is largely neglected. However, the critical state friction angle has been found dependent on the overall shape regularity in a mixture of angular sand and rounded glass beads [36, 55, 58]. This suggests the necessity to consider particle shape effect in conjunction with breakage. Consequently, the critical state strength and deformation are jointly contributed by the co-evolution of particle shape and particle size. A recent constitutive model proposed by [3] has introduced an interesting concept of shape attractor to consider the co-evolution of particle size and shape. A major assumption of the concept is that the average shape parameters of a crushable assembly may evolve toward a unique value at a critical or ultimate state, which apparently requires either experimental or numerical evidence to substantiate, e.g., the existence and/or uniqueness of shape attractors at critical state. In addition to grain size and shape, further consideration of fabric to characterize the critical state responses of crushable soils proves to be even challenging.

In this study, we employ a physics-based multiscale computational approach to conduct a comprehensive numerical investigation of the critical state behaviors of crushable granular sand under general stress conditions. Two critical issues are specifically addressed. *First*, the effect of particle crushing on the characteristics of CSLs and the evolutions of particle shape and anisotropy toward critical state. *Second*, the deformation mechanisms at critical state for crushable soils. The computational approach employed in the present study features hybridizing the non-smooth contact dynamics and peridynamics method, the former for simulating the granular system while the latter for modeling the breakage of individual particles. It enables rigorous treatments of grain size and shape co-evolution in granular media and thus suits well to tackle the said two issues. We also present a novel technique to decompose the volumetric strain and quantify the influence of particle size, particle shape, and frictional sliding on the deformation of crushable sand. Numerical studies simulating triaxial shear tests of crushable sand specimens with varying initial density, confining pressure, and loading path are systematically performed to capture the general critical state responses. A unified CSL incorporating the evolving particle size, shape, and fabric anisotropy is identified and compared with non-crushable counterparts, linking the macroscopic strength and

deformation with the interplays between reducing size and irregular shape at particle scale. The role of particle breakage on the deformation mechanisms at critical state and the competition between the void-filling and interlocking effect of child particles and the rearrangement effect of original particles are illustrated through a rigorous quantitative analysis. A transition point marking the dominance of crushing-induced contraction over frictional-induced dilation is identified, and a readily available parameter, crushing fraction, is proposed to distinguish the deformation modes at critical state. These observations help decode the fundamental critical state mechanisms in a novel way and facilitate the future development of more rigorous and general constitutive laws for crushable granular materials.

2 Methodology and numerical model

2.1 Multiscale modeling approach

A multiscale approach capable of simulating continuous grain crushing and tracking the co-evolution of particle size and shape proposed in [63, 64] is extended for general stress conditions to model the critical state behavior of crushable sand. The computational framework includes two major components:

- 1) Peridynamics (PD), a non-local mesh-free method specializing in modeling fracture-related problems in continuum media. In the peridynamic analysis, a solid material is discretized into material points connected by breakable bonds. A fracture surface forms after progressive breakage of the bonds. The PD method has gained increasing popularity in handling discontinuities since differentiation of the displacement field is replaced with integral functions in this method. In this study, the breakage of individual sand particles is modeled by an ordinary state-based PD theory through an open-source software Peridigm with a critical stretch damage model for the sand material [29, 38, 46].
- 2) Non-smooth contact dynamics (NSCD), an impulse-based iterative approach serving as an alternative to the classical discrete element method. In NSCD, particles are simulated as rigid bodies and the penetration between two contacting pairs is prohibited. The particle position, velocity, and inter-particle contact forces are updated based on the impulse between colliding bodies. This feature enables NSCD to handle large-scale granular systems with irregular particle shapes at ease and bypasses the complex algorithms for computing contact forces of irregular

shaped particles in the traditional penalty-based method [19, 44]. In NSCD, the contact detection and resolution process are conducted by solving the differential variational inequality coupled with equations of motion through an iterative solver. The discrete system is updated through the Euler semi-implicit linearized time integration scheme. In this study, the granular sand packing is simulated by NSCD with an open-source code Project Chrono [48].

The detailed coupling procedure between the two methods is illustrated in Fig. 1, and it can be summarized into the following three stages. The readers can refer to [63] for more details on the coupling and validation.

Stage 1: Screening of particles subject to breakage. At designated time steps (every 600 time steps in the NSCD analysis in this study), all the simulated particles are evaluated on their potential of breakage based on a maximum contact force (MCF) criterion [64]. Particles with a MCF exceeding a predefined threshold are screened for PD-based breakage analysis. The MCF criterion is employed in view of many previous studies indicating that single particle crushability is strongly correlated with the MCF exerted on it.

Stage 2: PD-based breakage analysis. The breakage analysis for selected particles in *Stage 1* is performed in a PD solver with a multi-thread parallel computing scheme to accelerate the computation. In the PD analysis, each particle is discretized into about 3,000 material points with an element size proportional to its equivalent diameter ($0.055d_e$). The horizon of a material point is set as 3 times of the element size. The boundary conditions applied in the PD analysis include contact position, contact normal, and inter-particle contact forces retrieved from the NSCD model. The contact forces are evenly distributed to material points within a contact radius of 2.5 times of the element size and are loaded at a constant rate of 1.6×10^6 N/s.

Stage 3: Child particle modeling. If a particle is found crushed in the PD analysis, it will be replaced by several polyhedron child particles occupying the same space in the NSCD system. The shape and position of child particles are retrieved from the PD analysis while the kinetic energy of child particles is assumed to be lost given the quasi-static conditions in the granular packing. The 3D alpha-shape method is adopted to generate the convex hulls of child particles from a cluster of PD material points. The base alpha shape value for child particles is 0.2 with an increment of 0.02 to ensure a polyhedron without self-intersection and singular face or edges. Child particles with a convexity larger than 0.85 or an equivalent diameter smaller than 1.0 mm are simplified into convex-shaped particles to avoid the time-consuming detection process for

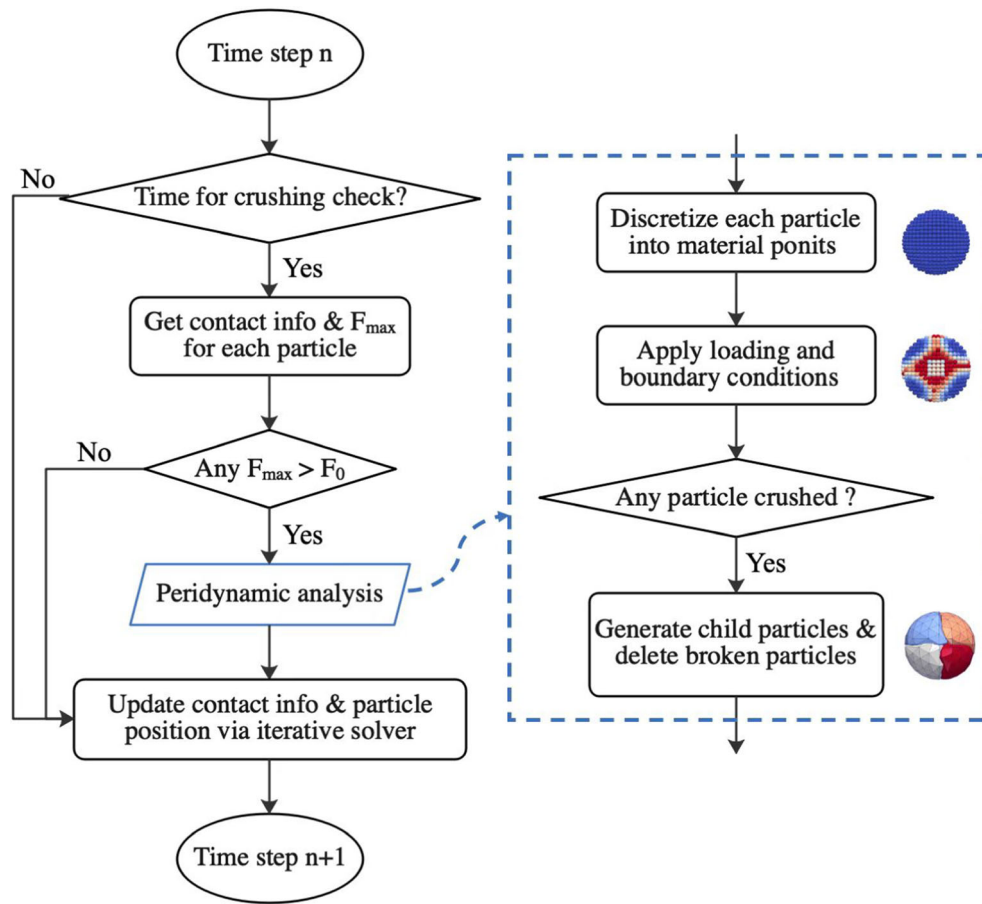


Fig. 1 Workflow of coupled non-smooth contact dynamics and peridynamics for modeling of crushable sand

concave particles. After receiving the child particles and reaching a new balance state, the NSCD system advances to the next time step. Stage 1 is repeated when it approaches the next designated time for particle breakage analysis.

2.2 Simulation of true triaxial shear of sand

A total number of 56 specimens are modeled, each containing an initial number of 5,000 mono-sized spherical particles with a diameter of 1.0 mm packed inside a cubic container with frictionless walls. In addition to the obvious computational efficiency, the use of mono-sized spherical particles for the initial packings offers a relatively clean and simple initial state to quantify the ensuing co-evolution of grain size and shape during the crushing process while avoiding the necessity of introducing extra parameters to describe the initial and critical state. Though packings with non-spherical particles and a grain size distribution that mimics natural sands may be more desirable, similar observations on the critical state characteristics can be expected as the idealized packings. Indeed, [40] have confirmed their classical critical state theory by testing data

on idealized granular media including glass beads and steel balls other than natural soils. The critical state behavior of sand with various initial gradings and shapes is also traceable from the results of mono-sized specimens [24]. The material properties of crushable sand in this study are summarized in Table 1. The simulated specimens cover a

Table 1 Properties of sand in this study

Parameters	Value
Young's modulus (GPa)	100
Poisson's ratio	0.15
Density (kg/m ³)	2,650
Initial void ratio	~ 0.60 (dense) ~ 0.75 (loose)
Critical energy release rate (J/m ²) (for a reference particle with $d = 1$ mm)	15
Weibull modulus	3.1
Inter-particle friction coefficient	0.3
Particle-boundary friction coefficient	0.0

combination of different initial void ratios (approximately 0.60 for dense specimen and 0.75 for loose specimen) and confining stresses ranging from 1.5 to 11 MPa. To consider general stress conditions where the intermediate stress plays a role, simulations are performed on specimens with different stress ratio b from 0 to 1, as well as specimens loaded with constant mean principal stress p' between 1.8 MPa and 9.0 MPa while keeping identical intermediate and minor principal stresses. All specimens are first isotropically compressed to predefined confining pressures. After consolidation, shearing is applied along the vertical z -axis to the specimen under three typical loading paths: triaxial compression, constant stress ratio b , and constant mean principal stress p' . The latter two quantities are defined by:

$$b = \frac{\sigma_2 - \sigma_3}{\sigma_1 - \sigma_3} \quad (1)$$

$$p' = \frac{\sigma_1 + \sigma_2 + \sigma_3}{3} \quad (2)$$

where σ_1 , σ_2 , and σ_3 are the major, intermediate, and minor principal stresses directly derived from reaction forces of the container walls, respectively. In constant b shearing, the confining pressure along the x -axis is kept constant while the stresses applied on the y -axis are continuously adjusted to maintain a constant b condition. To highlight the effect of grain crushing, benchmark cases are created by assuming particles to be non-crushable while all the other conditions are kept identical.

A servo control algorithm is adopted to guarantee the accuracy of applied stress and strain boundary conditions. All the specimens are sheared under a steady rate of 0.05 m/s, satisfying the quasi-static loading condition by maintaining an inertia number of 7.2×10^{-4} , which is well below the suggested threshold 2.5×10^{-3} [39]. The shearing is continued until classic critical state conditions with constant stress ratio and constant volumetric strain are asymptotically met. For samples under relatively large confining pressures (i.e., with more severe particle crushing), the constant volume criterion in determining the critical state condition is relaxed to a $\Delta\varepsilon_v/\Delta\varepsilon_1 < 0.05$ to render the computational time practical.

In the simulation, the strength of a particle is quantified by a material constant, critical energy release rate G_c , which is proportional to the square of characteristic particle strength following a Weibull distribution. Each particle is assigned with a unique G_c value following [34, 35]:

$$G_c = G_{c0}[-\ln(U(0, 1))]^{\frac{2}{\psi}} \left(\frac{V}{V_0}\right)^{-\frac{2}{\psi}} \quad (3)$$

where G_c and G_{c0} refer to the critical energy release rate of particles with a volume V and V_0 , respectively. The Weibull modulus ψ is set as 3.1 based on past experimental

studies [31, 35]. A reference G_{c0} is selected to be 15 J/m² for a spherical particle with $d = 1.0$ mm, which is found to yield reasonable uniaxial crushing strength in accordance with the literature [35]. Particle size is known to affect its strength as smaller particles contain fewer and smaller micro-cracks. Therefore, child particles generated due to breakage tend to be stronger than their mother particles. Such effect is considered by assigning a higher critical energy release rate for the child particles by the following:

$$G_{ch} = G_{pr} \left(\frac{V_{ch}}{V_{pr}}\right)^{-\frac{2}{\psi}} \quad (4)$$

where the subscript pr and ch refer to the relevant quantities of parent particles and child particles, respectively.

To enhance the computational efficiency, particles with an equivalent diameter smaller than 0.25 mm are not considered for further crushing, resembling a comminution limit for the modeled sand particles. A similar limiting particle size has been used by [16, 30, 32] in numerical studies of crushable sand, and the macroscopic behavior of their model is not influenced by the introduction of limiting particle size. Note that for natural sand there indeed exists a comminution limit [22] although the actual limit is much smaller than what is assumed here. To ensure the quasi-static loading condition during the compression, an unbalanced force ratio, defined by the ratio of unbalanced force to the average force magnitude on a particle, has been monitored throughout each simulation. The average unbalanced force ratio for all particles is kept below 1.5% to maintain good numerical stability and general equilibrium.

3 Critical state of crushable sand

3.1 Characteristics of CSL

In the numerical simulations, all the crushable samples are sheared to reach a critical state with steady deviator stress and constant volume at a relatively large axial strain level (typically after 60–70%) compared with their non-crushable counterparts (typical after 40–50%). The logarithmic strain and the Kirchhoff stress tensor are adopted in this study to quantify the stress–strain relationships at large deformation. Typical stress and strain relations of crushable sand sheared under various confining pressures are illustrated in Fig. 2 where the stress ratio, which we denote as η , is calculated by:

$$\eta = \frac{q}{p'} = M \quad (5)$$

where q represents the deviator stress obtained from:

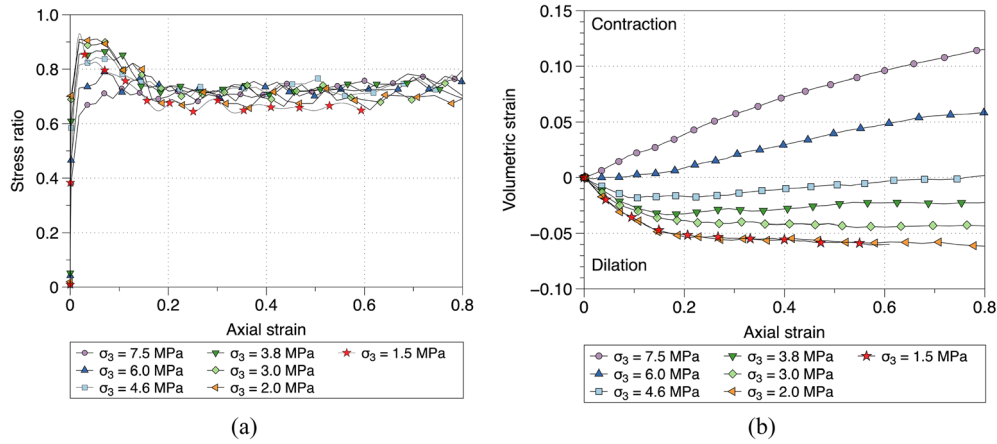


Fig. 2 Illustration of typical stress–strain relations obtained from numerical modeling under various confining pressures: (a) stress ratio versus axial strain; and (b) volumetric strain versus axial strain. For clarity purpose, not all data are presented

$$q = \sqrt{\frac{(\sigma_1 - \sigma_2)^2 + (\sigma_2 - \sigma_3)^2 + (\sigma_1 - \sigma_3)^2}{2}} \quad (6)$$

We first examine the CSL in the q - p' space by plotting the obtained deviatoric stress and mean principal stress of all specimens at critical state as shown in Fig. 3. In relatively low stress range (e.g., < 8 MPa), all results can be described with a linear relationship with high credibility ($R^2 > 0.991$) regardless of the stress path and initial void ratio. The slope of this linear correlation signifies the critical state stress ratio M_c and it is found to be 0.781 for crushable sand specimens. The linear correlation between p'_c and q_c with constant M_c has been acknowledged in many existing experimental and numerical results [37, 45, 50] Nonetheless, for specimens subject to very large p'_c (e.g., above 10 MPa) the resulting critical stress ratio appears to be slightly higher. To assess the severity of particle crushing in the specimens at different stress levels,

Harding’s breakage index [15] for all specimens at critical state is included in the figure. It is apparent that specimens with large p'_c experience more severe fragmentation. The implication is that increasing particle crushing leads to a higher critical state stress ratio M_c . The comparison cases with non-crushable particles are also presented in Fig. 3. Notably, the non-crushable specimens exhibit a rather consistent and smaller M_c regardless of stress levels. The difference in M_c between non-crushable and crushable cases at small stress levels appears to be negligible whereas it is markable at high stress levels. A higher M_c in the crushable case at high stresses generally implies a higher strength at critical state. The observation thus suggests that particle crushing may help enhance soil strength at high confinements. Such an effect may arise from the increasing fine particles produced after significant breakage events, which fill the voids and spread out the contact forces that were originally concentrated. Meanwhile, the irregularity of fragments helps strengthen the interlocking effect and leads to higher soil strength [14, 61].

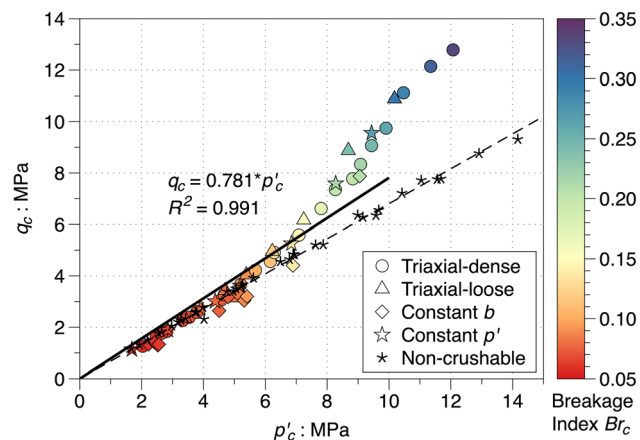


Fig. 3 Effect of grain crushing on critical state line (CSL) in q - p' space. q_c and p'_c represent the deviatoric stress and mean principal stress at critical state, respectively

The critical state mean principal stress p'_c is known to be uniquely correlated with void ratio e_c and [25] suggested an exponential correlation between e_c and p'_c which writes:

$$e_c = e_{\Gamma} - \lambda_e \left(\frac{p'_c}{p_a} \right)^{\zeta} \quad (7)$$

where e_{Γ} refers to the critical state void ratio at zero pressure ($p'_c = 0$). λ_e and ζ are material constants, and $p_a = 101$ kPa denoting the atmospheric pressure. Note that when $\zeta = 1.0$, Eq. (7) degenerates into a linear equation. The correlation between e_c and p'_c obtained from the simulations is presented in Fig. 4 for both crushable and non-crushable sand specimens. Evidently, a bi-linear relation of e_c and p'_c for crushable sand is observed. It can be well described by Eq. (7) with $e_{\Gamma 1} = 0.776$, $\lambda_{e1} = -0.015$, and $\zeta = 1.0$ for $p'_c < 4.5$ MPa and $e_{\Gamma 2} = 1.02$,

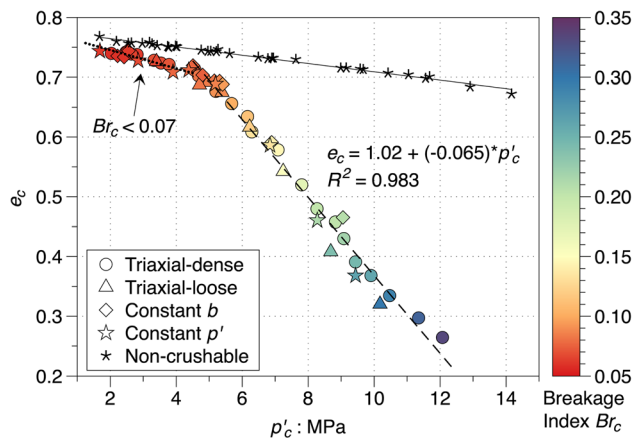


Fig. 4 Effect of grain crushing on CSL in e - p' space

$\lambda_{e1} = -0.065$, and $\xi = 1.0$ for $p'_c > 4.5$ MPa. The observation is consistent with previous experimental and numerical observations [6, 24, 33]. Different loading paths achieved by varying b and p' have little effect on the CSL in the e - p' space. Under low confining stress conditions (e.g., $p'_c < 4.5$ MPa), there is very limited particle breakage as reflected by the low breakage index, and the CSLs for both crushable and non-crushable sand are indistinguishably close. However, the CSL for crushable sand exhibits a clear transition $p'_c = 4.5$ MPa beyond which the influence of grain crushing becomes apparent. Increasing particle breakage leads to a downward shift of CSL in e - p' space. The turning point also signifies the transition of soil response from dilative to contractive to achieve critical state as shown in Fig. 2b. At very large mean principal stresses (e.g., $p'_c > 12$ MPa), the CSL appears to bend toward the horizontal direction, possibly due to the imposed crushing limit which prevents further breakage of already fine particles. A three-stage conceptual model for crushable soils has been proposed in the literature [33, 41] with the introduction of two transition points to account for the onset and cessation of significant particle crushing events respectively. Nonetheless, assuming a bi-linear relationship between e_c and p'_c is considered appropriate practically since extremely large stress conditions are uncommon in a typical geotechnical engineering context.

The relationship between mean principal stress p'_c and Hardin's breakage index Br_c at critical state is also examined. The breakage index signifies the degree of particle breakage in a granular assembly. It is quantified by the ratio of change in particle size distribution before and after shearing. The critical state breakage index Br_c versus mean stress is plotted in Fig. 5a. Again, a bi-linear relationship is identified with a turning point at around $p'_c = 4.5$ MPa. Particle breakage is intensified with p'_c above this stress level with an apparent increase in the breakage index with rising p'_c . In view of the unique relevance of e - p' and Br

p' , an evident correlation of the three quantities can be derived in the form of a spatial curve as reported by some experimental and numerical studies [6, 37, 54, 62].

It is worth noting that particle crushing does not cease to occur even after critical state is reached. As shown in Fig. 5b, the breakage index continues to increase at a constant rate when a general definition of critical state with constant stress and volume has been maintained over a sustained deformation stage. The ring shear tests conducted by [9] also confirm that breakage continues to occur at extremely large shear strains far beyond the normal range of conventional triaxial tests. Since particle crushing still exists and its influence on assembly volume is not negligible at critical state, a question is raised pertaining to how the constant volume condition is attained in the presence of crushing-induced volumetric contraction. To answer this question, a strain decomposition method will be introduced later to explore the fundamental critical state mechanisms influenced by noticeable particle crushing.

3.2 Critical state particle shape

In addition to the degrading particle size originating from breakage, the evolution of particle shape constitutes an important aspect in the process of particle breakage. In the present study, we employ two popular particle shape factors, namely sphericity and aspect ratio, to evaluate particle shape evolution of the granular media. The sphericity measures the deviation of an irregular-shaped particle from a perfect sphere. It is calculated by $\Psi = \sqrt[3]{36\pi V_p^2/A_p}$ where V_p and A_p refer to the volume and surface area of a particle, respectively. The aspect ratio is calculated as the ratio of the shortest dimension to the longest dimension of a particle.

As shown in Fig. 6a, b, a unique relation between the median value of the sphericity Sph_{50} or the aspect ratio AR_{50} of an assembly and the mean principal stress p'_c can be delineated at critical state. Due to the scarcity of crushed particles, the sphericity and aspect ratio for specimens sheared under lower stresses exhibit larger fluctuations but still fall within a narrow range. The median aspect ratio evolves quickly and stays nearly unchanged near 0.58. This observation supports the recent theory proposed by [3] that a stable particle shape profile can be obtained at critical state or at the end of particle crushing, and the ultimate particle shape distribution can be evaluated by single or multiple shape attractors. Expectedly, the median sphericity exhibits a similar evolution pattern. Nonetheless, our results show that the median sphericity appears to evolve slower and continues to show a slightly decreasing trend in the modeled stress levels, indicating the formation of more irregularly shaped particles inside the assembly. A

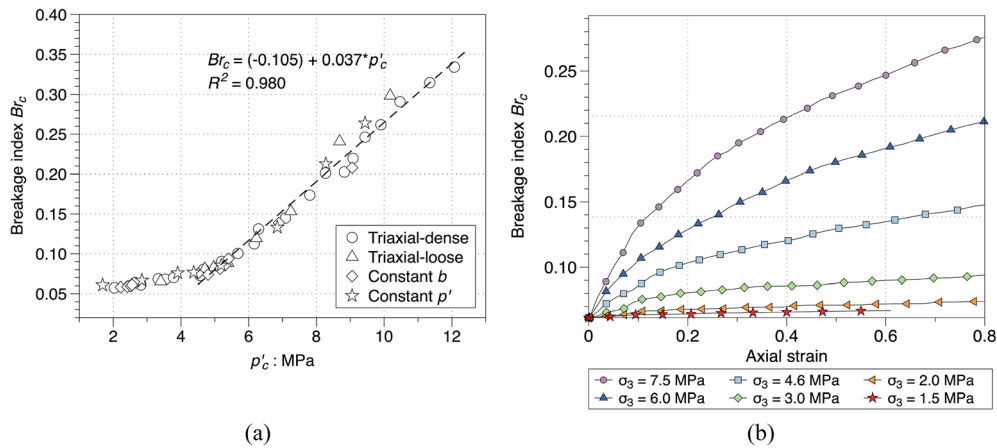


Fig. 5 (a) Correlation of critical breakage index Br_c with mean stress p'_c at critical state; and (b) Evolution of Br_c for specimens sheared under different confining pressures

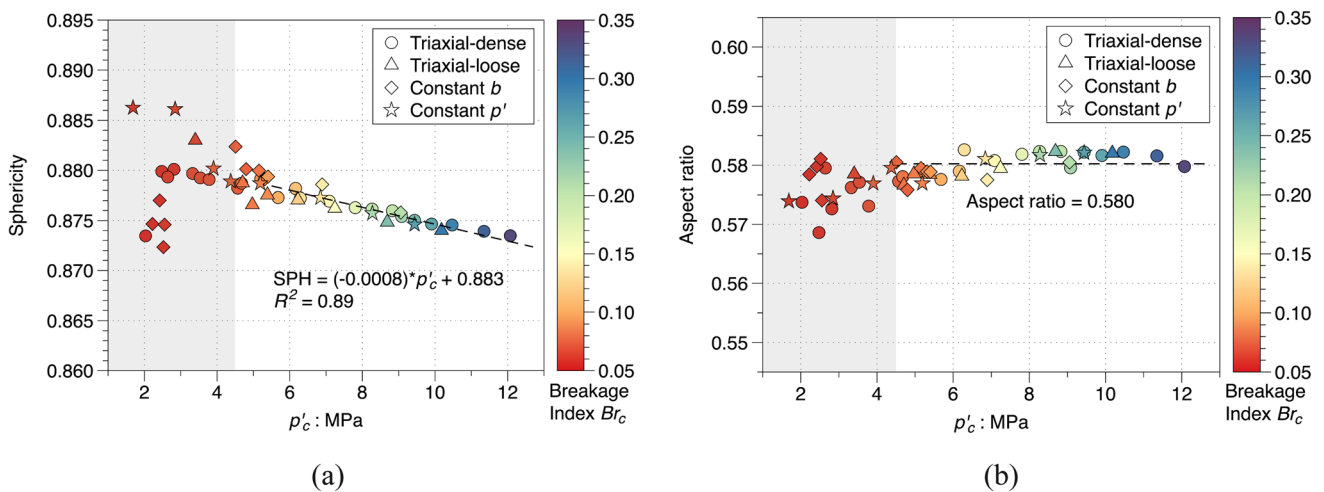


Fig. 6 (a) Correlation of critical state sphericity and (b) critical state aspect ratio AR with mean principal stress p'_c

comparison with other experiments and numerical simulations indicates that all the critical state shape factors are located near a certain point as shown in the Zingg diagram Fig. 7a which are comparable to the ultimate shape of nature sands [4, 11, 21, 43, 49, 65]. A further investigation into the particle shape distribution of a triaxial compression test in Fig. 7b reveals that massive child particles are generated with a less regular shape, resembling plates or rods. The irregular particle shapes are expected to enhance the interlocking between particles, resulting in a dilative volumetric response and this effect will be discussed later.

3.3 Critical state fabric anisotropy

It is instructive to extract further micromechanical information from the simulation results to gain insights into the critical state behavior of granular media. The study is further extended to probe into the influence of particle

crushing on the critical state fabric anisotropy for crushable sand. The degree of fabric anisotropy A_c is calculated through the second invariant of the contact normal tensor Φ_{ij} , as defined by:

$$\Phi_{ij} = \frac{1}{N_c} \sum_{c \in N_c} n_i n_j \tag{8}$$

$$a_{ij}^c = \frac{15}{2} \Phi'_{ij}, A_c = \sqrt{\frac{3}{2}} a_{ij}^c a_{ij}^c \tag{9}$$

where n_i and n_j are the unit vector along the i -th and j -th direction of contact normal. N_c refers to the total number of contacts within the assembly and Φ'_{ij} is the deviatoric part of the fabric tensor Φ_{ij} .

We take an example by using cases with $b = 0.0$ and constant p' , at different initial void ratios and confining pressures, to examine the correlation between A_c and p' at critical state as shown in Fig. 8a. All the specimens exhibit an overall anisotropic response at critical state. A unique

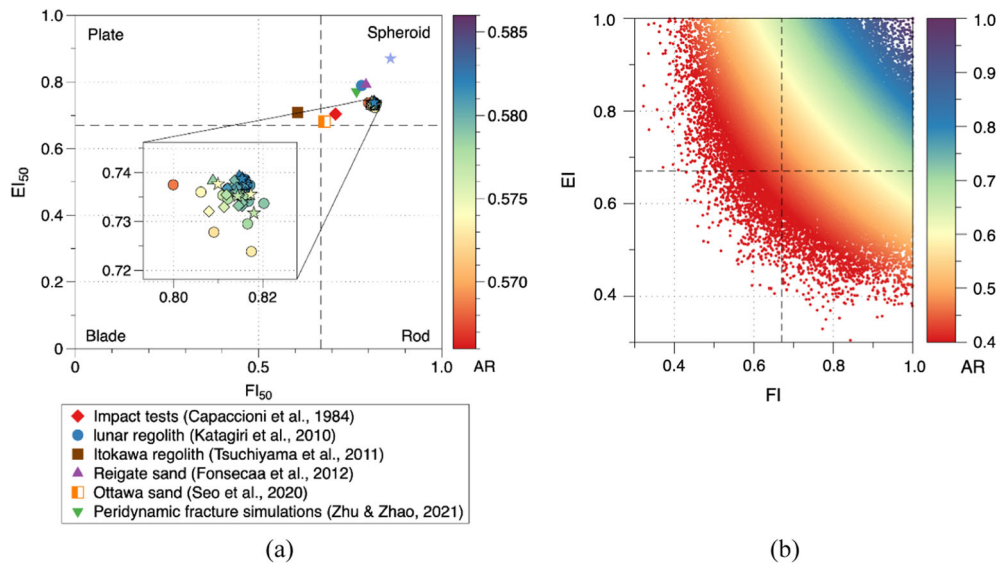


Fig. 7 Zingg diagrams of: (a) the median values of particle shape factors at critical state from experimental and numerical results and (b) shape factors for all particles within an assembly at $b = 0.0$, $\sigma_3 = 11$ MPa

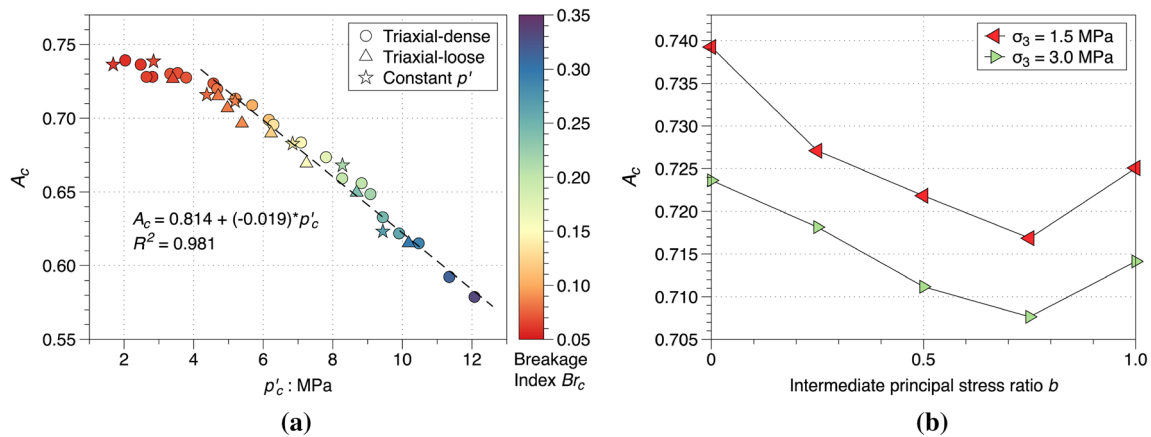


Fig. 8 Correlation of critical state fabric anisotropy A_c with (a) mean stress and (b) intermediate principal stress ratio at critical state

fabric anisotropy line is observed independent of the initial fabric and stress conditions. However, a further examination reveals that the intermediate principal stress ratio b influences the fabric anisotropy as shown in Fig. 8b which suggests that the A_c is indeed loading path dependent. The results for other b values are not presented here for clarity. It is worth noting that the same phenomenon has also been reported for non-crushable sand [13, 51].

The correlation between A_c and p' exhibits a typical bilinear trend differentiated by the degree of crushing, consistent with the behaviors of critical state void ratio, breakage index, and shape factors presented above. The fabric anisotropy shows a high level for slightly crushed specimens and drops with increasing p' . As the mean principal stress rises, more breakage events take place, and the fabric anisotropy experiences an accelerated reduction

in magnitude due to the increasing polydispersity brought by particle crushing, making the assembly more isotropic.

4 Deformation mechanisms at critical state

The deformation of crushable sand is a combined result of several interacting mechanisms. The crushing of particles reduces particle size and the generated fine fragments fill the inter-particle voids, yielding a more compacted specimen. Meanwhile, the continuous breakage of particles creates irregular shape particles which tend to strengthen the interlocking effect and cause dilation. The two mechanisms compete during the shearing, playing distinctive roles in dominating the overall deformation of crushable granular media at different loading stages. Additionally, the inter-particle frictional sliding also contributes to the

overall deformation of the specimen. These mechanisms are schematically illustrated in Fig. 9.

A total of 12 representative cases are selected to study the deformation mechanism of crushable sand. In the selected cases, sand specimens are sheared under varying stress levels (p'_c ranging from 2.0 to 10.4 MPa), loading paths (constant b and constant p' tests), and initial states (dense and loose packings). We introduce a new approach to decompose the volumetric strain of the specimen into three parts, including a size-reduction induced strain (size effect), a particle shape related strain (shape effect) due to the interlocking effect, and a frictional sliding induced strain (friction effect), to offer a quantitative probing into the deformation mechanism of crushable granular sand.

4.1 Strain decomposition

The deformation of the specimens at critical state is evaluated through a logarithmic form of volumetric strain ε_v to describe large strain deformation with improved accuracy [13], and it is defined as:

$$\varepsilon_v = \int d\varepsilon_v = \int_V^{V_0} \frac{dV}{V} = \ln \frac{V_0}{V} \quad (10)$$

where V_0 and V are the specimen volume at initial and critical state, respectively. Contraction is taken as positive. The volumetric strain increment $\Delta\varepsilon_v$ is then derived from the differences of ε_v between two adjacent time intervals. A strain decomposition method similar to the parallel probe

approach [5, 47] is adopted to differentiate the strain increment components contributed by grain crushing from total strains. The total incremental strain $\Delta\varepsilon_v$ can be seen as the sum of the following three components:

$$\Delta\varepsilon_v = \Delta\varepsilon_f + \Delta\varepsilon_{size} + \Delta\varepsilon_{shape} \quad (11)$$

where $\Delta\varepsilon_f$ represents the effect from sliding and rearrangement of the remaining unbroken particles due to inter-particle friction. This effect exists even without particle crushing and accounts for the dilative behavior for a dense packing and contractive behavior for a loose packing. $\Delta\varepsilon_{size}$ denotes the contractive void-filling effect due to particle size reduction. $\Delta\varepsilon_{shape}$ is the shape effect that reflects the volume change brought by the interlocking and rearrangement of particles with irregular shapes. The latter two components originate from the particle crushing process.

To evaluate each of the strain increment components, three parallel analyses are run to measure the volumetric strains for each case. They include:

- i) A standard triaxial shear where particle breakage is enabled throughout the simulation (crushable specimen). This analysis simulates the actual condition of crushable granular sand to provide the total volumetric strain increment $\Delta\varepsilon_v$.
- ii) A comparison model which assumes all particles are non-crushable (non-crushable specimen). For

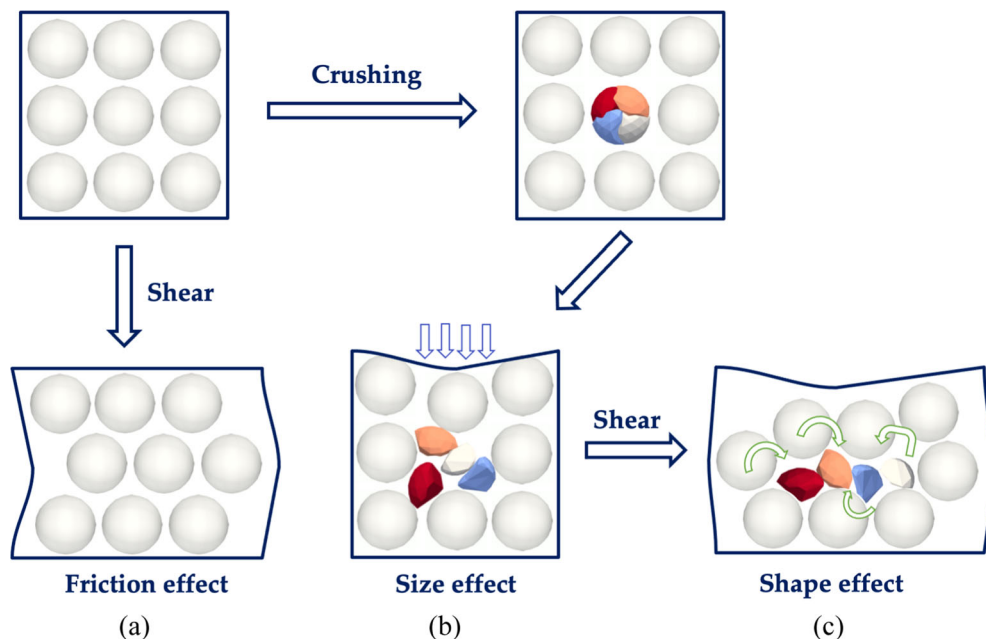


Fig. 9 Schematic illustration of different mechanisms in the volumetric strain of crushable granular media: (a) inter-particle friction, (b) size reduction induced deformation, and (c) particle shape effect on deformation

subtraction gives the incremental size effect during the incremental axial strain of $\Delta\varepsilon_1$. The incremental size effect $\Delta\varepsilon_{size}$ can then be calculated by

$$\Delta\varepsilon_{size} = (\Delta\varepsilon_v - \Delta\varepsilon_{NCk})|_{at\varepsilon_1=k+\Delta\varepsilon_1} \quad (13)$$

where $\Delta\varepsilon_v$ is the total strain increment of the crushable specimen and $\Delta\varepsilon_{NCk}$ is the total strain increment of the partially crushable specimen of “NC_k”, both measured at the strain level between k and $k + \Delta\varepsilon_1$. Summing up the strain increment during the loading process gives the total strain due to the size effect. The axial strain increment $\Delta\varepsilon_1$ is taken to be 5% in the present study. For each case, 12–16 strain probes are typically run in parallel at different axial strains. The selected strain interval contains approximately two crushing check intervals to ensure that sufficient crushing events are captured and that the influence of grain crushing on the deformation of the specimen is identifiable. Taking smaller increments is expected to offer more accurate results but at a much higher computational cost since a reference model “NC_k” has to be run at each strain increment. Finally, the shape effect can be found by subtracting the size-induced and friction-induced strain obtained above from the total strain.

4.2 Size and shape effect on deformation

For crushable sand, the volumetric strain induced by the size reduction and shape effect can be prominent. With the strain decomposition approach introduced earlier, a quantitative assessment of each deformation mechanism is now possible. We first examine the volumetric strain due to the size effect for specimens at different confining pressures, with data presented in Fig. 11a. The size effect is found to cause a sustained contraction of the specimen. The stress condition is found to exert a significant influence on the size effect. For specimens sheared under mild stress conditions (e.g., $\sigma_3 = 3.5$ MPa), the size effect remains

limited. At higher stresses, however, considerable volumetric contraction is found upon shearing. The severity of the size effect is positively related to the confining stress. To give a better quantification of particle crushing under different stress levels, we introduce a quantity termed crushing fraction defined by the mass ratio of crushed particles to the specimen. In the numerical simulation, it is convenient to extract the crushing fraction in any strain intervals for the evaluation of particle crushing rate. For the present study, the crushing fraction of the specimen at each incremental axial strain of approximately 2% is plotted in Fig. 12. The incremental strain can of course be selected at other values at the convenience of the study. It can be observed that higher stress levels result in a higher crushing fraction which lasts until large strains. Consequently, the size effect on the volumetric strain is therefore, more significant under high stress levels.

The volumetric strain originating from the shape effect is plotted in Fig. 11b. This effect is attributed to the rearrangement and interlocking of child particles and is found to be dilative in general. Once particle crushing occurs, the child particles tend to have higher shape irregularities than the initial spherical particles and the interlocking effect is strengthened thereby. As an overall observation, the shape effect tends to be stronger with higher stress levels.

4.3 Competition of the deformation mechanisms

The ultimate deformation of the crushable sand results from the competition of the three deformation mechanisms. The present study is further extended to examine the evolution of each mechanism during the loading process for the 12 selected specimens where different loading conditions and initial states are covered. The relative proportions of the three volumetric strain components are presented in Fig. 13 for those cases. Notably, the dominating mechanism of deformation varies significantly with stress levels

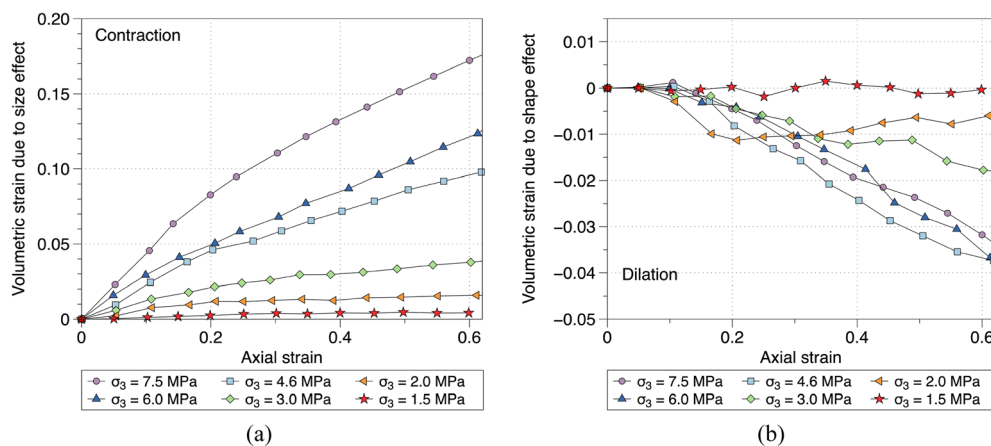


Fig. 11 Evolution of (a) size effect and (b) shape effect on the volumetric strain of the specimen

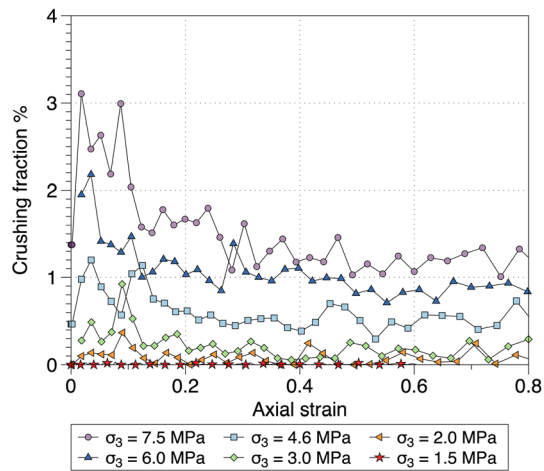


Fig. 12 Evolution of crushing fraction versus axial strain. The fraction of crushing indicates the mass ratio of particles that experience crushing in an incremental axial strain

and initial state. In general, the deformation mode of those cases can be classified into three categories: (1) friction-dominated dilation, (2) size effect dominated contraction, and (3) dilation aroused by competing mechanisms. They are discussed in detail in the following.

The friction-dominated deformation (Fig. 13a) is typically found in specimens under relatively low stress conditions with limited particle crushing. The contraction caused by the size-reduction effect is noticeably less than the dilation brought by the frictional rearrangement of particles in the initial packing. Therefore, an overall dilatative response can be expected. In this case, the crushable sand specimens bear similar strength, deformation, and fabric properties to non-crushable ones.

For size effect dominated deformation (Fig. 13b), significant particle damage occurs under elevated stress conditions (e.g., $p'_c > 5.5$ MPa for the studied specimen). Increasing fine fragments are generated to fill the voids. The crushing-induced contraction accumulates gradually to cancel out the dilation caused by the inter-particle friction and shape effect. A transition of volumetric strain from dilation to contraction can be identified due to the stronger size effect under increasing p' . For specimens subjected to high mean stresses, the size effect plays a leading role and generates an immediate contraction upon shearing. The mechanical behaviors of those highly crushable specimens are distinct from the non-crushable counterparts due to an increasing proportion of child particles participating in strong force chains. The influence of the original particles on the strength and deformation of the entire packing is weakened. Therefore, the friction effect contributed by the rearrangement of original particles becomes less significant while the size and shape effects keep strengthening at large shear strains. At critical state, a counterbalance is formed

between the increasing contraction from space-filling of fine particles and the dilatancy originating from the child particle interlocking effect. If the specimen is sheared under extremely high confining pressures, the dilative shape and friction effect may be overwhelmed by the significant size effect caused by the massive fine particles produced from crushing. Under this circumstance, a typical critical state is hard to achieve within the scope of triaxial tests, as the specimen may keep contracting without approaching an apparent steady state.

A transitional zone is found at intermediate stress levels (e.g., $p'_c = 3.0$ to 5.5 MPa in this study) where none of the three mechanisms has an absolute advantage over the others (Fig. 13c). For specimens categorized into the transitional zone, the friction, size, and shape effect act together to achieve a constant volume condition. A general dilatative response is observed before achieving a constant volume condition at critical state for this zone. Noticeably, the size and shape effect keep evolving even at the critical state while the friction effect becomes stabilized in advance. Sustained particle breakage events are still found within the packings with a moderate crushing fraction (e.g., at around 0.1%) even after the critical state is reached, resulting in fine fragments filling the voids and irregularly shaped particles maintaining the interlocking effect.

A further investigation on the effect of initial density is conducted with specimens having initially loose packing. Results are presented in Fig. 13d. A more contractive response arising from the conversion of friction effect from dilation to contraction is observed in those loose specimens. The initial loose state accommodates enough space for the original particles to rearrange and form a more efficient packing to resist the external loadings. Therefore, the frictional rearrangement of original particles makes the packing less dilatant or contractive. The effects of size and shape are less influenced by the initial density than the friction effect and their contributions to the overall deformation of a specimen are correlated with the average stress levels. For specimens located at friction-dominant or transitional regimes, the contractive friction effect plays a decisive role in specimen deformability while under increased confining pressures, the influence of initial density is less remarkable but adds to the degree of contraction at critical state.

It is worth mentioning that the shape effect may become contractive in exceptional circumstances. This is observed in an initially loose specimen under a large confining pressure of 12 MPa as shown in Fig. 13d. A possible explanation for this behavior is that particle crushing tends to dominate throughout the deformation process under very high stress levels. The interlocking effect cannot be fully developed as the particles break easily. The contractive shape effect observed herein can be understood as the

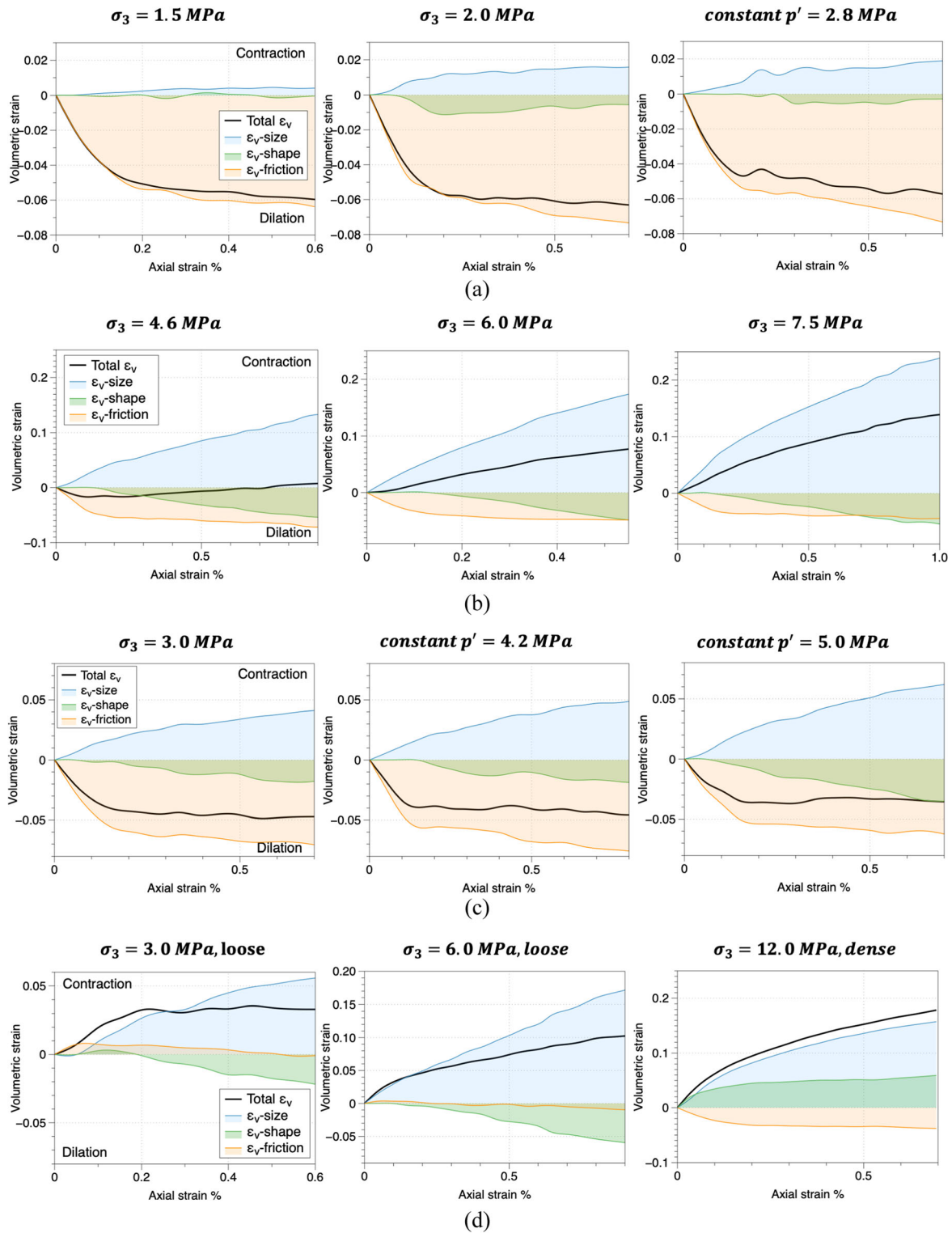


Fig. 13 Proportion of size, shape, and frictional effect under different stress conditions (a) Friction-dominant deformation with small mean principal stress; (b) Size-dominant deformation with large mean principal stress; (c) Competing friction, size, and shape effect with intermediate mean principal stress; (d) Deformation of initially loose and highly contractive specimens

tendency to produce irregular particles that are easier to break and cause contraction, rather than producing the interlocking effect that contributes to dilation. Indeed, the

continuous particle crushing process produces many particles with small elongation and flatness as shown in Fig. 7b. These particles are expected to bear relatively low

strength and break easily during the sustained shearing [65, 66].

4.4 Critical state conditions

Based on the above analyses, the critical state conditions for crushable granular sand can be classified into three categories based on the dominating deformation mechanism. As presented in Fig. 14, the CSL in the $e-p'$ space spans three zones of different deformation modes: the friction-dominant, size effect dominant, and balanced size-shape effect. The different deformation mechanisms are differentiated according to the mean stress levels at critical state. For specimens located in the friction-dominant area, an overall dilative volumetric strain is anticipated during shearing due to the predominance of friction effect from original particles and limited influence of particle crushing. The stress levels at the transition from friction dominant zone to balanced size-shape effect zone indicate the onset of a moderate level of particle crushing. For moderately crushable specimens, a less dilative response is observed due to the growing size effect. The transition to size effect dominant zone indicates the presence of significant particle crushing. For highly crushable specimens, the deformation is governed by the overwhelming size effect due to significant particle breakage under elevated stresses. A fast-growing breakage index (e.g., $Br_c = 0.1-0.35$) and a stable particle shape profile are maintained.

Using stress levels to gauge the deformation mode can be material and loading-path dependent. A material that contains stronger/weaker grains is expected to experience mode transition at higher/lower stress levels. The crushing fraction per incremental axial strain introduced earlier seems to be a better quantity to gauge the mode of deformation at the critical state. In all the studied cases, a small crushing fraction ($< 0.25\%$) appears to indicate a friction-dominated deformation mode. A crushing fraction of about 0.4% marks the transition into size effect dominated deformation mode. An extremely large crushing fraction (e.g., $> 1.4\%$) makes it challenging to balance the three mechanisms as the contractive size effect prevails over the dilative friction and shape effect, which is stabilized at a moderate crushing fraction. Nonetheless, the case with a very large crushing fraction is expected to be uncommon in a typical geotechnical engineering context. It would be interesting to explore further whether the crushing fraction can be used as a universal criterion to gauge deformation mode for a wide variety of crushable granular materials. This is beyond the scope of the present work and needs further study from both numerical and experimental aspects.

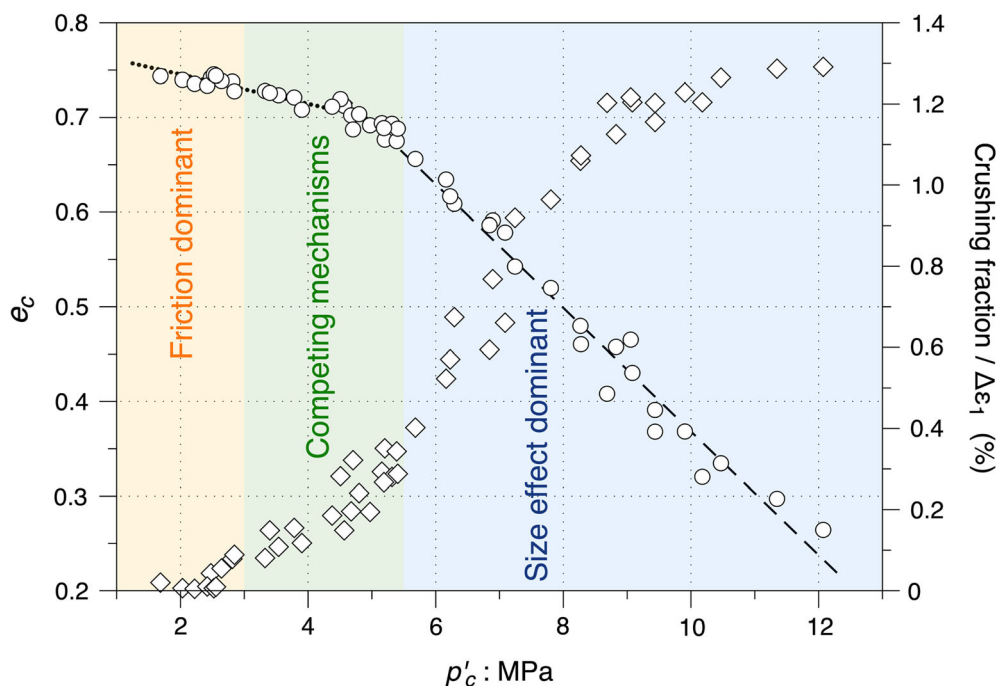


Fig. 14 The deformation mechanisms at critical state for crushable sand specimens under various stress states. The crushing fraction indicates the mass ratio of crushed particles to the specimen at each axial strain increment of approximately 2%

5 Conclusions

This study offers a comprehensive study of the critical state mechanisms of crushable granular sand based on a multi-scale computational approach. A series of true triaxial tests with various stress paths and initial densities are modeled to systematically investigate the influence of particle crushing on the critical state behavior of sand. A novel strain decomposition approach is proposed to quantitatively examine three mechanisms underpinning the macroscopic deformation of crushable granular media. They include size-reduction induced contraction, interlocking between irregular shape particles which leads to dilation, and frictional effect of particles before crushing. The study offers new insights into the critical state mechanisms involving the entangled mechanisms brought by particle crushing. The major findings are summarized as follows:

(1) A unique void ratio e_c , breakage index Br_c , and sphericity Sph_c regardless of stress condition, loading path, and initial density can be identified at the critical state for crushable granular sand. A unique stress ratio M_c also exists for all specimens studied under small stress ranges. At high stress range when particle crushing is prominent, the stress ratio M_c tends to be higher. The critical state fabric anisotropy A_c is found to be loading path dependent.

(2) With the increase of mean effective stress p' , particle crushing has a more significant impact on the critical state behaviors with a strengthened critical state stress ratio and a bending of CSL in e - p' space. There exists a critical stress level beyond which the dominance of particle breakage is observed in CSL correlating p'_c and the critical state void ratio, breakage index, sphericity, and fabric anisotropy.

(3) The study confirms the persistent occurrence of particle crushing at critical state. The constant volume condition of a crushable sand packing may be maintained by the interplays between the contractive size arising from finer grain size, the dilative shape, and the friction effect driven by the inter-particle friction, sliding, and interlocking due to the increasing irregularities of child particles.

(4) The critical state deformation of crushable sand can be categorized into three distinct modes: friction-dominant dilation, size effect-dominant contraction, and a transition state in between. The crushing fraction, which defines the mass ratio of the crushed particles to the specimen during an incremental strain, may be used as an indicator to gauge the mode of deformation at the critical state.

Our findings shed light on the signature behaviors of crushable sand at critical state and their underlying deformation mechanisms. Future challenges and possible

improvements for the numerical and constitutive modeling of crushable granular materials rest in the following respects: (1) Specially designed apparatus capable of shearing specimens to hundreds of shear strains are required to delineate CSLs of different scopes at extremely high stress states where the crushing fraction maintains a high level; (2) More varieties on the initial grading, initial density, and loading paths (such as undrained and cyclic shearing) are expected to fully capture the critical state responses of crushable sand specimens; (3) All packings in our numerical simulations are loaded under a quasi-static condition where the dynamic effect is neglected. A further examination of the particle fracture patterns and stress-strain relations under dynamic loadings or impacts is needed to assess the potential consequence of more severe particle breakages in these conditions.

Acknowledgements The study was financially supported by National Natural Science Foundation of China (under Project 11972030), Research Grants Council of Hong Kong (GRF #16208720), and the Project of Hetao Shenzhen-Hong Kong Science and Technology Innovation Cooperation Zone (HZQB-KCZYB-2020083). The first author acknowledges financial support from Hong Kong Ph.D. Fellowship Scheme funded by Research Grants Council of Hong Kong. Data for all figures are available from the corresponding author upon reasonable request. The authors appreciate the constructive comments raised by both anonymous reviewers.

References

- Bandini V, Coop MR (2011) The influence of particle breakage on the location of the critical state line of sands. *Soils Found* 51(4):591–600
- Bolton MD (1987) Discussion: the strength and dilatancy of sands. *Géotechnique* 37(2):219–226
- Buscarera G, Einav I (2021) The mechanics of brittle granular materials with coevolving grain size and shape. *Proc R Soc A* 477(2249):20201005
- Capaccioni F, Cerroni P, Coradini M, Farinella P, Flamini E, Martelli G et al (1984) Shapes of asteroids compared with fragments from hypervelocity impact experiments. *Nature* 308(5962):832–834
- Ciantia MO, Arroyo M, Calvetti F, Gens A (2016) A numerical investigation of the incremental behavior of crushable granular soils. *Int J Numer Anal Meth Geomech* 40(13):1773–1798
- Ciantia MO, Arroyo M, O'Sullivan C, Gens A, Liu T (2019) Grading evolution and critical state in a discrete numerical model of fontainebleau sand. *Géotechnique* 69(1):1–15
- Cil MB, Hurley RC, Graham-Brady L (2020) Constitutive model for brittle granular materials considering competition between breakage and dilation. *J Eng Mech* 146(1):04019110
- Coop, M. R., & Lee, I. K. (1992). The behaviour of granular soils at elevated stresses. Paper presented at the Predictive Soil Mechanics: Proceedings of the wroth memorial symposium held at St Catherine's college, Oxford, pp 186–198.
- Coop MR, Sorensen KK, Bodas Freitas T, Georgoutsos G (2004) Particle breakage during shearing of a carbonate sand. *Géotechnique* 54(3):157–163

10. Dafalias YF, Taiebat M (2016) SANISAND-Z: Zero elastic range sand plasticity model. *Géotechnique* 66(12):999–1013
11. Fonseca J, O’Sullivan C, Coop MR, Lee PD (2012) Non-invasive characterization of particle morphology of natural sands. *Soils Found* 52(4):712–722
12. Gao Z, Zhao J (2017) A non-coaxial critical-state model for sand accounting for fabric anisotropy and fabric evolution. *Int J Solids Struct* 106:200–212
13. Guo N, Zhao J (2013) The signature of shear-induced anisotropy in granular media. *Comput Geotech* 47:1–15
14. Guo P, Su X (2007) Shear strength, interparticle locking, and dilatancy of granular materials. *Can Geotech J* 44(5):579–591
15. Hardin BO (1985) Crushing of soil particles. *J Geotech Eng* 111(10):1177–1192
16. Hanley KJ, O’Sullivan C, Huang X (2015) Particle-scale mechanics of sand crushing in compression and shearing using DEM. *Soils Found* 55(5):1100–1112
17. He SH, Goudarzy M, Ding Z, Sun Y (2023) Strength, deformation, and particle breakage behavior of calcareous sand: role of anisotropic consolidation. *J Geotech Geoenviron Eng* 149(3):04023002
18. Houlsby GT (1991) How the dilatancy of soils affects their behaviour. University of Oxford, Oxford
19. Jean M (1999) The non-smooth contact dynamics method. *Comput Methods Appl Mech Eng* 177(3–4):235–257
20. Jefferies M, Been K (2015) Soil liquefaction: a critical state approach. CRC Press, Boca Raton
21. Katagiri J, Matsushima T and Yamada Y (2010) Statistics on 3D particle shapes of lunar soil (no. 60501) obtained by micro X-ray CT and its image-based DEM simulation. *Earth and space 2010: engineering, science, construction, and operations in challenging environments*, pp 254–259
22. Kendall K (1978) The impossibility of comminuting small particles by compression. *Nature* 272:710–711
23. Leung CF, Lee FH, Yet NS (1997) The role of particle breakage in pile creep in sand. *Can Geotech J* 33(6):888–898
24. Li G, Liu Y, Dano C, Hicher P (2015) Grading-dependent behavior of granular materials: from discrete to continuous modeling. *J Eng Mech* 141(6):04014172
25. Li XS (1997) Modeling of dilative shear failure. *J Geotech Geoenviron Eng* 123(7):609–616
26. Li XS, Dafalias YF (2012) Anisotropic critical state theory: role of fabric. *J Eng Mech* 138(3):263–275
27. Liu Y, Liu X, Hu W (2023) Competition mechanism between dilation and interlocking in granular soils: DEM simulation and constitutive modeling. *Acta Geotech* 18(1):149–169
28. Luzzani L, Coop MR (2002) On the relationship between particle breakage and the critical state of sands. *Soils Found* 42(2):71–82
29. Madenci E, Oterkus E (2014) *Peridynamic theory. Peridynamic theory and its applications*. Springer, Singapore, pp 19–43
30. Marketos G, Bolton MD (2009) Compaction bands simulated in discrete element models. *J Struct Geol* 31(5):479–490
31. McDowell GR (2002) On the yielding and plastic compression of sand. *Soils Found* 42(1):139–145
32. McDowell GR, de Bono JP (2013) On the micro mechanics of one-dimensional normal compression. *Géotechnique* 63(11):895–908
33. Muir Wood D, Maeda K (2008) Changing grading of soil: Effect on critical states. *Acta Geotech* 3(1):3–14
34. Nakata A, Hyde M, Hyodo H, Murata. (1999) A probabilistic approach to sand particle crushing in the triaxial test. *Géotechnique* 49(5):567–583
35. Nakata Y, Hyodo M, Hyde AF, Kato Y, Murata H (2001) Microscopic particle crushing of sand subjected to high pressure one-dimensional compression. *Soils Found* 41(1):69–82
36. Nie JY, Zhao J, Cui YF, Li DQ (2021) Correlation between grain shape and critical state characteristics of uniformly graded sands: a 3D DEM study. *Acta Geotech* 56:1–16
37. Ning F, Liu J, Kong X, Zou D (2020) Critical state and grading evolution of rockfill material under different triaxial compression tests. *Int J Geomech* 20(2):04019154
38. Parks ML, Littlewood DJ, Mitchell JA and Silling SA (2012) *Peridigm users’ guide v1. 0.0*. SAND Report, 7800.
39. Perez JL, Kwok CY, Huang X, Hanley KJ (2016) Assessing the quasi-static conditions for shearing in granular media within the critical state soil mechanics framework. *Soils Found* 56(1):152–159
40. Roscoe KH, Schofield A, Wroth AP (1958) On the yielding of soils. *Géotechnique* 8(1):22–53
41. Russell AR, Khalili N (2004) A bounding surface plasticity model for sands exhibiting particle crushing. *Can Geotech J* 41(6):1179–1192
42. Schofield AN, Wroth P (1968) *Critical state soil mechanics*. McGraw-hill, London
43. Seo D, Sohn C, Cil MB, Buscarnera G (2021) Evolution of particle morphology and mode of fracture during the oedometric compression of sand. *Géotechnique* 71(10):853–865
44. Servin M, Wang D, Lacoursière C, Bodin K (2014) Examining the smooth and nonsmooth discrete element approaches to granular matter. *Int J Numer Meth Eng* 97(12):878–902
45. Shi DD, Cao D, Deng YB, Xue JF (2021) DEM investigations of the effects of intermediate principal stress ratio and particle breakage on the critical state behaviors of granular soils. *Powder Technol* 379:547–559
46. Silling SA, Epton M, Weckner O, Xu J, Askari E (2007) Peridynamic states and constitutive modeling. *J Elast* 88(2):151–184
47. Tamagnini C, Calvetti F, Viggiani G (2005) An assessment of plasticity theories for modeling the incrementally nonlinear behavior of granular soils. In: Tamagnini C (ed) *Mathematics and mechanics of granular materials*. Springer, Dordrecht, pp 265–291
48. Tasora, A., Serban, R., Mazhar, H., Pazouki, A., Melanz, D., Fleischmann, J., et al. (2015). Chrono: An open source multi-physics dynamics engine. Paper presented at the international conference on high performance computing in science and engineering, pp 19–49
49. Tsuchiyama A, Uesugi M, Matsushima T, Michikami T, Kadono T, Nakamura T et al (2011) Three-dimensional structure of hayabusa samples: origin and evolution of itokawa regolith. *Science* 333(6046):1125–1128
50. Ventouras K, Coop MR (2009) On the behaviour of thanet sand: an example of an uncemented natural sand. *Géotechnique* 59(9):727–738
51. Wen Y, Zhang Y (2022) Evidence of a unique critical fabric surface for granular soils. *Géotechnique* 14:1–16
52. Wiebicke M, Andò E, Viggiani G, Herle I (2020) Measuring the evolution of contact fabric in shear bands with X-ray tomography. *Acta Geotech* 15(1):79–93
53. Wroth CP (1958) *The behaviour of soils and other granular media when subjected to shear*. Doctoral dissertation, University of Cambridge, Cambridge.
54. Xiao Y, Liu H, Ding X, Chen Y, Jiang J, Zhang W (2016) Influence of particle breakage on critical state line of rockfill material. *Int J Geomech* 16(1):04015031
55. Xiao Y, Long L, Matthew Evans T, Zhou H, Liu H, Stuedlein AW (2019) Effect of particle shape on stress-dilatancy responses of medium-dense sands. *J Geotech Geoenviron Eng* 145(2):04018105
56. Yamamuro JA, Lade PV (1996) Drained sand behavior in axisymmetric tests at high pressures. *J Geotech Eng* 122(2):109–119

57. Yan WM, Dong J (2011) Effect of particle grading on the response of an idealized granular assemblage. *Int J Geomech* 11(4):276–285
58. Yang J, Wei LM (2012) Collapse of loose sand with the addition of fines: the role of particle shape. *Géotechnique* 62(12):1111–1125
59. Yilmaz Y, Deng Y, Chang CS, Gokce A (2021) Strength–dilatancy and critical state behaviours of binary mixtures of graded sands influenced by particle size ratio and fines content. *Géotechnique* 25:1–16
60. Zhao J, Guo N (2013) Unique critical state characteristics in granular media considering fabric anisotropy. *Géotechnique* 63(8):695–704
61. Zhao S, Zhou X (2017) Effects of particle asphericity on the macro-and micro-mechanical behaviors of granular assemblies. *Granul Matter* 19(2):1–18
62. Zhong W, Yue F, Ciancio A (2018) Fractal behavior of particle size distribution in the rare earth tailings crushing process under high stress condition. *Appl Sci* 8(7):1058
63. Zhu F, Zhao J (2019) Modeling continuous grain crushing in granular media: a hybrid peridynamics and physics engine approach. *Comput Methods Appl Mech Eng* 348:334–355
64. Zhu F, Zhao J (2019) A peridynamic investigation on crushing of sand particles. *Géotechnique* 69(6):526–540
65. Zhu F, Zhao J (2021) Interplays between particle shape and particle breakage in confined continuous crushing of granular media. *Powder Technol* 378:455–467
66. Zhu F, Zhao J (2021) Multiscale modeling of continuous crushing of granular media: The role of grain microstructure. *Comput Particle Mech* 8(5):1089–1101

Publisher's Note Springer Nature remains neutral with regard to jurisdictional claims in published maps and institutional affiliations.

Springer Nature or its licensor (e.g. a society or other partner) holds exclusive rights to this article under a publishing agreement with the author(s) or other rightsholder(s); author self-archiving of the accepted manuscript version of this article is solely governed by the terms of such publishing agreement and applicable law.